


Article

Significant Reduction in Precipitation Seasonality and the Association with Extreme Precipitation in the Hai River Basin of China from 1960 to 2018

Xin Zhang ¹  and Yuna Mao ^{2,*}¹ School of Environment, Beijing Normal University, Beijing 100875, China; xzhang0828@mail.bnu.edu.cn² State Key Laboratory of Earth Surface Processes and Resource Ecology, Faculty of Geographical Science, Beijing Normal University, Beijing 100875, China

* Correspondence: myn@bnu.edu.cn

Abstract: The Hai River Basin (HRB) serves as a vital center for the population, economy and politics in northern China. Natural hazards, particularly floods, pose significant risks to the region, often attributed to extreme precipitation events. Changes in precipitation seasonality play a pivotal role in influencing precipitation extreme events. Therefore, this study presents a comprehensive analysis of precipitation seasonality and its impact on precipitation extremes in HRB. By implementing a novel relative entropy method, we calculated the precipitation seasonality indicators using daily precipitation observations from 1960 to 2018 in HRB. We found a significant decreasing trend in precipitation seasonality ($-0.03 \text{ decade}^{-1}$, $p = 0.04$), accompanied by an earlier onset date (4.0 days decade^{-1} , $p = 0.01$) and longer duration (4.3 days decade^{-1} , $p = 0.03$) of the wet season. Notably, these trends are notably concentrated in the Beijing-Tianjin administrative regions. Additionally, a lower precipitation seasonality value indicated a more evenly distributed precipitation throughout the year, resulting in reduced occurrences of precipitation extremes. Consistently, we observed two precipitation extremes, extreme wet day precipitation R99T and maximum 1-day precipitation RX1Day, which exhibited significant decreasing trends at the rate of $-0.5 \text{ mm decade}^{-1}$ ($p = 0.02$) and $-1.4 \text{ mm decade}^{-1}$ ($p = 0.05$), respectively. Furthermore, we detected significant positive correlations of 0.31 ($p = 0.02$) and 0.35 ($p = 0.01$) between precipitation seasonality and precipitation extremes (R95T and R99T), suggesting that a more evenly distributed precipitation across seasons corresponds to fewer precipitation extremes over the past sixty years. Metropolitan areas, in particular, experienced a noteworthy reduction in precipitation seasonality and a decreased frequency of precipitation extreme events. The findings of this study shed new light on the intricate relationship between precipitation seasonality and extreme events, further helping policy making develop effective risk regulations for agriculture, floods, and urban waterlogging, ensuring sustainable development within the HRB.

Keywords: gauge observations; precipitation seasonality; precipitation extreme events; Hai River Basin

Citation: Zhang, X.; Mao, Y. Significant Reduction in Precipitation Seasonality and the Association with Extreme Precipitation in the Hai River Basin of China from 1960 to 2018. *Atmosphere* **2023**, *14*, 1552. <https://doi.org/10.3390/atmos14101552>

Academic Editor: Corene Matyas

Received: 17 August 2023

Revised: 5 October 2023

Accepted: 10 October 2023

Published: 11 October 2023



Copyright: © 2023 by the authors. Licensee MDPI, Basel, Switzerland. This article is an open access article distributed under the terms and conditions of the Creative Commons Attribution (CC BY) license (<https://creativecommons.org/licenses/by/4.0/>).

1. Introduction

Global warming is primarily caused by human activities, particularly fossil fuels burning in production systems [1–4]. The intensification of extreme precipitation is a well-known consequence of global warming [5–11]. It has been estimated that the global surface temperature will rise by 1.4–5.8 degrees at the end of the 21st century, resulting in an increase in both the frequency and intensity of extreme precipitation [12–15]. The Intergovernmental Panel on Climate Change (IPCC, 2021) [16] has reported that extreme precipitation events have been increasing since 1951 in many mid-latitude regions, despite a decreasing trend observed in total annual precipitation [16]. Additionally, the area experiencing more frequent and intense extreme precipitation in the middle and high latitudes of the northern hemisphere is expanding [17]. Given the potential for increased

flooding risks, it is crucial to pay careful attention to the intensification of precipitation, as it can have devastating consequences for both human societies and the environment [18–20].

Numerous studies have illustrated that changes in extreme precipitation are likely to be greater than those in mean precipitation under a warmer climate [21]. There is also heterogeneity in the trends of increasing frequency and intensity of extreme precipitation events under climate warming [6,11,22]. For example, recent research conducted in China found that the total amount of precipitation at annual and seasonal scales has increased, accompanied by an increase in the intensity and frequency of extreme precipitation from 1960 to 2018, except in the northern region of China [23,24]. These findings are consistent with previous results that reported an increase in the extreme precipitation in western and southern China, while a decreasing trend was observed in northern China [25–27]. The precipitation extreme events, defined as the tail of the distribution, are influenced by both a shift in the mean and a change in variability [28,29]. Several studies reported that the increase in variability is similar in magnitude to the increase in mean precipitation, even larger in some cases [30–32].

Under a warmer climate, not only the frequency and intensity of extreme precipitation events were affected, but also precipitation patterns, such as a delayed phase in the seasonal cycle of precipitation [33–36], a redistribution of rainfall from early to late in the monsoon season [37], and changes in precipitation seasonality [24,38]. In monsoon regions, a shortened wet season coupled with increased rainfall may significantly increase the frequency and intensity of precipitation events. The decrease in precipitation seasonality can be mainly attributed to a lower concentration of rainfall during the wet season, reduced annual rainfall, and an earlier onset of the wet season.

Precipitation seasonality, a complex concept that consists of many components, including magnitude, timing, and duration of the wet season [39,40], is particularly suitable for analyzing seasonality in regions with uneven distribution of annual rainfall [41,42]. For example, the regions with a strengthened seasonality are expected to experience higher precipitation magnitude, which will occur on the very rainy-day events referred to as extreme precipitation events. Hence, the spatial and temporal pattern of precipitation seasonality and its impact on the extent of extreme precipitation provides a new perspective for analyzing the potential driving forces of precipitation extreme events.

The Hai River Basin (HRB), the largest river in North China, sustains the highest population density with the lowest per capita water resource availability in China [43]. In this study, we aimed to conduct a comprehensive analysis of the spatial–temporal pattern of precipitation characteristics in HRB, such as magnitude and timing, duration of the wet season, and the pattern of precipitation seasonality and precipitation extremes and their links. Understanding these patterns is of importance for comprehending the changes in runoff patterns, and effectively managing the flood risk within the basin. Using daily precipitation data from gauge stations in the Hai River Basin from 1960 to 2018, our study employed seasonality indicators of precipitation, associated with the characteristics of precipitation extreme indices, to describe their patterns and long-term tendencies and the connections between the precipitation seasonality and precipitation extremes.

2. Data and Methods

2.1. Study Area

The Hai River Basin (HRB) is one of the major river basins in China, covering an area of about 318,200 square kilometers. It is located in northern China and includes parts of several provinces and municipalities, including Hebei, Beijing, Tianjin, Shanxi, and Inner Mongolia. The population in HRB is over 124 million.

The hydrology of the HRB is characterized by a temperate monsoon climate, with distinct wet and dry seasons. Surface water resources in the Hai River Basin are primarily derived from precipitation and runoff. The basin is fed by various tributaries, such as the Luan River, the Ziya River, and the Wei River. These tributaries converge with the main stem of the Hai River, forming a complex network of rivers and streams.

2.2. Data

The ground-based daily precipitation data are obtained from the China National Stations Fundamental Elements Datasets V3.0 (<http://data.cma.cn>, accessed on 30 September 2021) that covered ~2400 rain gauge stations from 1960 to 2018. Rigorous quality control, including spatiotemporal consistency checks, extreme value checks, and corrections of suspected erroneous values, has been applied to the datasets [44] and is regarded as the latest meteorological dataset with good quality and integrity and applied to many studies [45–47]. The 143 precipitation stations are evenly distributed in the Hai River Basin, as shown in Figure 1.

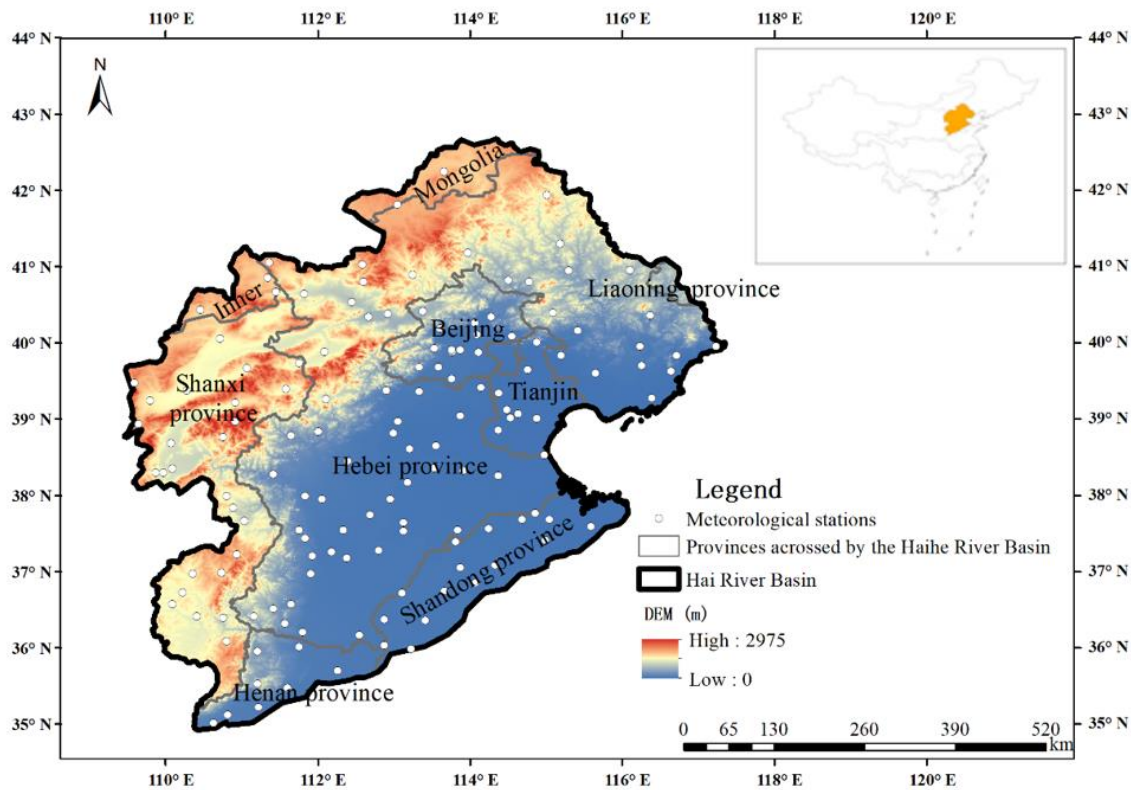


Figure 1. The distribution of meteorological gauge stations in the Hai River Basin. The inset map indicates the location of the Hai River Basin in China (yellow). The daily precipitation anomaly is calculated by subtracting mean daily precipitation from daily precipitation records.

2.3. Methods

2.3.1. Characterization of Precipitation Seasonality

To characterize the precipitation seasonality regime for the river basin, the following basic features were considered: onset date and cessation date of the wet season, duration of the wet season, the total amount of precipitation, and intensity in the wet season.

As illustrated in Figure 2, the climatological daily precipitation and the cumulative precipitation anomaly from 1960 to 2014 were calculated. The onset and cessation of the wet season were defined by the minimum and maximum value of cumulative precipitation anomaly. The total precipitation amount and the intensity during the wet season at each station were obtained as:

$$r_{total,k} = \sum_{i=onset}^{cessation} r_{i,k}$$

$$I_k = \frac{r_{total,k}}{D}$$

where $r_{total,k}$ is the total precipitation during the wet season, I_k The intensity of precipitation in the wet season was calculated by $r_{total,k}$ divided by the wet season duration D . The wet season duration is the period between the onset and cessation dates.

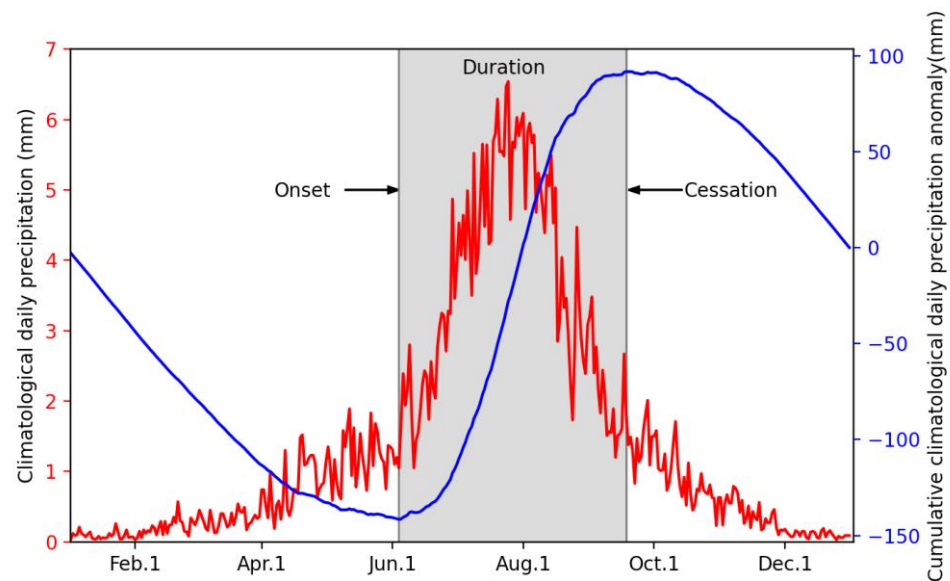


Figure 2. The schematic illustration of the definition including onset date, cessation date, and duration of the wet season in HRB. The daily precipitation anomaly is calculated by subtracting mean daily precipitation from daily precipitation records.

2.3.2. Seasonality Index

The seasonality index (SI) is an indicator to describe the extent of rainfall concentration during the wet season. A high SI represents a higher degree of seasonal variation in precipitation and a low SI indicates a relatively even distribution pattern of rainfall in a year. The calculation of SI in each year is followed by Feng et al. [41]:

$$SI_k = \sum_{m=1}^{12} p_{m,k} \log_2 \frac{p_{m,k}}{q_m}$$

$$p_{m,k} = \frac{r_{m,k}}{r_k}$$

where SI_k is the seasonality index, $r_{m,k}$ is the monthly precipitation in each year k , $p_{m,k}$ is the proportion of monthly precipitation accounting for annual precipitation r_k and q_m is the value of 1/12 representing uniformly distributed precipitation across 12 months.

The theory of SI provides a quantitative concentration of precipitation and has been applied widely for studies on global and local seasonality characterizers and changes [24,27,38–40].

2.3.3. Extreme Precipitation Indices

The annual precipitation extremes are calculated based on the daily time series of precipitation from 1960 to 2018. Six indices, including annual maximum 1-day and 5-day precipitation, extreme wet day precipitation, and the number of heavy precipitation days have been considered to evaluate the precipitation extreme events, based on Expert Team on Climate Change Detection and Indices (ETCCDI) (http://etccdi.pacificclimate.org/list_27_indices.shtml, accessed on 14 March 2023). The definitions of those indices are listed:

1. $R \times 1Day_j$ (mm), annual maximum 1-day precipitation, calculated by

$$R \times 1Day_j = \max(RR_{ij})$$

where RR_{ij} is the daily precipitation amount on the day i in the year of j .

2. $R \times 5Day_j$ (mm), annual maximum 5-day precipitation, calculated by

$$R \times 5Day_j = \max(RR_{kj})$$

where RR_{kj} is the precipitation amount for 5-day interval ending k in the year of j .

3. R10mm (day), the number of heavy precipitation days, calculated by an annual count of days when daily precipitation is more than 10 mm.
4. R25mm (day), the number of very heavy precipitation days, calculated by the annual count of days when daily precipitation is more than 25 mm.
5. R95T (mm), very wet daily precipitation, calculated by annual total precipitation when $RR > 95$ th:

$$R95T = \sum_{w=1}^W RR_{wj} \text{ where } RR_{wj} > RR_{wn95}$$

where RR_{wj} is the daily precipitation amount on a wet day w ($RR \geq 0.1$ mm) in the year j and RR_{wn95} is the 95th percentile of precipitation on wet days in the year 1960–2018. W represents the number of wet days in the year j .

6. R99T (mm), extreme wet daily precipitation, calculated by annual total precipitation when $RR > 99$ th:

$$R99T = \sum_{w=1}^W RR_{wj} \text{ where } RR_{wj} > RR_{wn99}$$

where RR_{wj} is the daily precipitation amount on a wet day w ($RR \geq 0.1$ mm) in the year j and RR_{wn99} is the 99th percentile of precipitation on wet days in the year 1960–2018. W represents the number of wet days in the year j .

2.3.4. Trends Analysis

The long-term trend of variables (precipitation seasonality indices and extreme events) was detected by a common nonparametric method, the Mann–Kendall trend test, combined with Sen's slope. The two methods are usually applied together and have been widely applied to many climate-analysis studies [48–51]. The Pearson correlation coefficient was employed for the connection between precipitation extremes and the seasonality index to study the interannual variability of precipitation annual time series.

3. Results

3.1. The Spatial–Temporal Pattern of Precipitation Seasonality Components

The spatial patterns of precipitation seasonality components have been shown in Figure 3, including the start and cessation dates and the length of the wet season, the magnitude of annual and wet season precipitation, and the seasonality index. A different pattern of wet season onset (cessation) dates and duration happened between the east and west parts of HRB (Figure 3a–c). Notably, the wet season started in May and ended in October in the western basin, while it started in June and ended in September in the eastern basin. Generally, the onset dates of the wet season were gradually delayed but earlier cessation dates of the wet season from the west to the east. Accordingly, an obvious temporal difference in duration was illustrated in Figure 3c that the duration was below 110 days in the eastern basin, and over 130 days in the western basin. From Figure 3d,e, we found the peak precipitation during the wet season happened in the northern basin,

approximately 85 mm, while the minimum precipitation was found in the southern basin with a value of 60 mm. In contrast, the intensity of precipitation during the wet season in the eastern basin was at least 1.5 times higher than in the western basin.

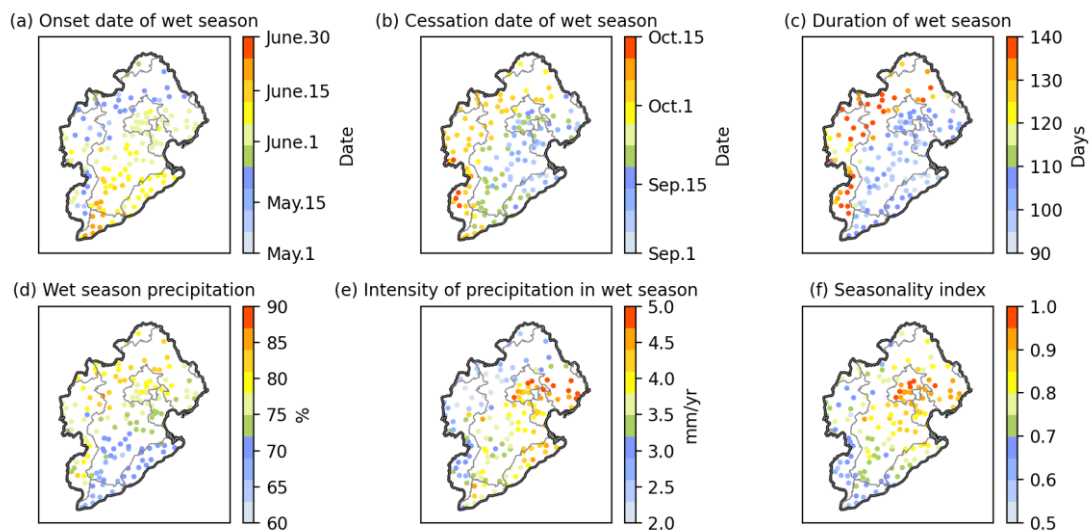


Figure 3. The spatial distribution of multiyear mean precipitation seasonality components at gauge stations from 1960 to 2018: (a) onset date of the wet season, (b) cessation date of the wet season, (c) duration of the wet season, (d) the ratio of wet season precipitation to annual precipitation, (e) intensity of wet season precipitation and (f) seasonality index.

Similarly, the seasonality index exhibited a spatial pattern similar to the intensity of precipitation during the wet season that an increasing magnitude of the seasonality index and intensity from west to east was shown with the higher value prominently concentrated in the metropolises of Beijing and Tianjin. However, compared to the precipitation intensity in the wet season, the seasonality index showed a smooth transition from the western to eastern zones. The Beijing administrative region exhibited the highest seasonality index in the basin, approximately 0.9–1. Stations with high seasonality index had a shorter duration of the wet season, as the pattern of the seasonality index was highly consistent with the time and duration of the wet season. Furthermore, the stations with the highest seasonality index did not correspondingly manifest the highest amount of wet season precipitation season, as shown in Figure 3d–f. This pattern highlighted the heterogeneity characterizing precipitation distribution over a year, particularly within metropolis domains.

3.2. The Interannual Variability and Long-Term Trends in Precipitation Seasonality Components

The spatial pattern of the precipitation seasonality components trends over the past 59 years is illustrated in Figure 4. A significant decreasing trend in the onset dates of the wet season was observed at the basin-wide scale, with an average decrease of -0.2 day yr^{-1} . Notably, the earliest trends were observed within the Beijing administrative region at a significant rate of -0.4 day yr^{-1} . The stations with the opposite trends in cessation dates were distributed in the southern and northern parts of the basin (Figure 4b): delayed cessation dates in the northern basin, particularly in the Beijing administrative region (0.3 day yr^{-1}), and conversely the decreasing trends in the southmost basin (a significant 0.4 day yr^{-1}). Consequently, the duration of the wet season exhibited an increasing tendency of greater than 0.43 day yr^{-1} from 1960 to 2018 (Figure 4c), and the stations within the Beijing administration region showed notably larger trends in the length of the wet season, approximately a significant 1 day yr^{-1} .

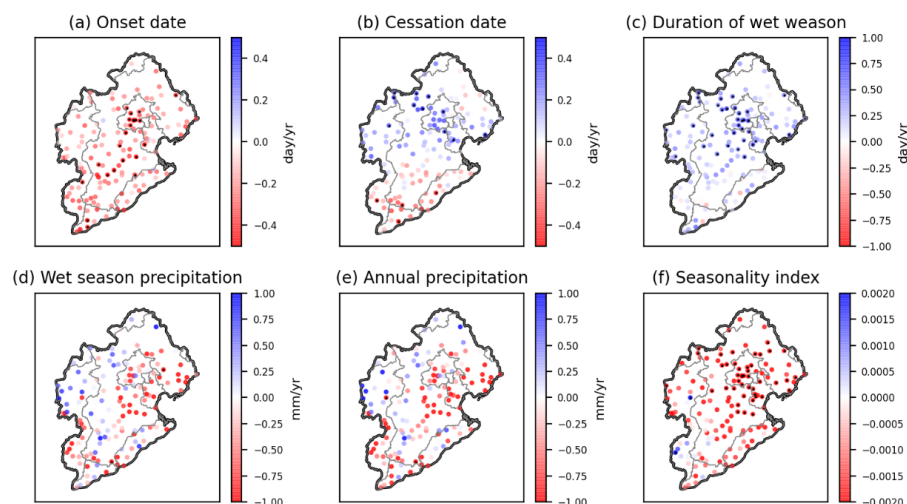


Figure 4. Long-term trends of precipitation seasonality components at gauge stations from 1960 to 2018: (a) onset date of the wet season; (b) cessation date of the wet season; (c) duration of the wet season; (d) the total amount of precipitation during the wet season; (e) the annual amount of precipitation; (f) seasonality index. The blue circles represent the increasing trends and the red circles represent the decreasing trends. The black dots filled in blue or red circles represent the significance at a confidence level of 95%.

As shown in Figure 4d,e, a similar spatial pattern of long-term trends was found in wet season precipitation and annual precipitation, both of them showing no significant changes. However, an obvious decrease was mainly concentrated in the Beijing and Tianjin regions. At the basin-wide scale, the stations exhibited a decreasing tendency in seasonality, with the significant trends particularly concentrated in the Beijing and Tianjin administrative regions, with a significant rate of -0.002 yr^{-1} .

Figure 5 indicated the interannual variations and trends of annual precipitation seasonality components at a basin-wide scale from 1960 to 2018. The variability of precipitation during the wet season showed consistency with the fluctuations in annual precipitation (Figure 5a,e): a slight decrease during the period of 1976–1980, followed by an increase from 1997 to 2018. Both annual precipitation and wet season precipitation exhibited slight insignificant decrease trends, with a rate of -0.32 mm yr^{-1} and -0.54 mm yr^{-1} , respectively. In terms of the onset date and the duration of the wet season, the heightened interannual variability during the period of 1981–2018 was exhibited compared to 1960–1980. As shown in Figure 5b,d, the onset date showed a significantly decreasing trend ($-0.40 \text{ day yr}^{-1}$) during the period of 1960–2018, whereas the cessation date displayed no obvious changes, resulting in a slightly longer trend of the wet season duration (0.43 day yr^{-1}). Hence, we inferred a longer wet season with a slightly decreasing trend of annual precipitation over the past 59 years. This deduction was also verified by the variability and the trend of the seasonality index: the tendency of the seasonality index was a significant -0.003 per year. The spatial pattern of seasonality index trends, combined with the duration of the wet season, indicated that even precipitation distribution happened over the year across HRB when the wet season was prolonged, especially significantly concentrating within metropolis regions.

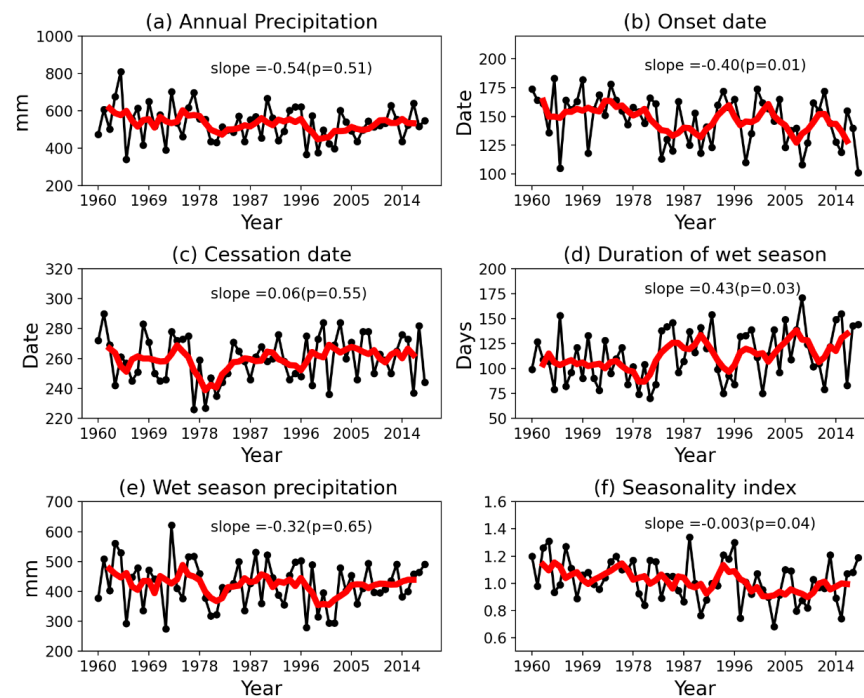


Figure 5. The interannual variability of six precipitation seasonality indices and their trends at a basin-wide scale from 1960 to 2018 in HRB: (a) annual precipitation; (b) onset date of the wet season; (c) cessation date of the wet season; (d) the duration of the wet season; (e) the precipitation amount during the wet season; (f) seasonality index. The black dot line represents the annual time series of precipitation seasonality indices and the thick red line represents the 5-year moving average of each index.

3.3. The Interannual Variability and Long-Term Trends of Precipitation Extremes

Over the period of 1960–2018, we assessed the long-term trends of precipitation extremes, including RX1Day, RX5Day, R95T, R99T, R10mm, and R25mm across each station within the HRB, as shown in Figure 6. Notably, the trends of RX1Day, RX5day, R95T, and R99T at the basin-wide scale showed similar spatial patterns, albeit with varying magnitudes. These extreme indices exhibited obvious decreasing trends in the Beijing and Tianjin administration regions, approximately at a rate of -0.3 mm yr^{-1} (RX1Day), -0.5 mm yr^{-1} (RX5Day), -0.75 mm yr^{-1} (R95T), and -0.4 mm yr^{-1} (R99T), respectively. In contrast, the stations with increasing trends in these extremes indices were much fewer, mostly distributed along the edge of the basin.

Compared to other precipitation extremes indices, the number of stations with significant trends of R10mm and R25mm was relatively small, as shown in Figure 6e,f. In particular, R10mm showed an increasing trend near the Beijing administration region, while 12 stations showed a decreasing trend located in the easternmost part of the basin. Compared with R10mm, only 10 stations showed decreasing trends in R25mm, with 5 of them located close to Beijing at a rate of $-0.01 \text{ day yr}^{-1}$. Notably, the R10mm and R25mm demonstrated the opposite tendencies in the Beijing administration region that the heavy precipitation days increased while the extreme heavy precipitation days decreased from 1960 to 2018.

Figure 7 illustrated the temporal pattern of precipitation extremes, including RX1Day, RX5Day, R95T, R99T, R10mm, and R25mm from 1960 to 2018. From Figure 7a,d, RX1Day and R99T exhibited significant decreasing trends, with the values of $-0.14 \text{ day yr}^{-1}$ ($p = 0.05$) and $-0.05 \text{ day yr}^{-1}$ ($p = 0.02$), respectively. RX1Day had a small fluctuation from 1960 to 2011, followed by a sharp increase in 2012. The highest value for RX1Day, reaching 90 mm, was found in 2016. In contrast, R99T exhibited substantial variability from 1960 to 1975, with a maximum value of 210 mm in 1963. RX5Day and R95T had no

significant tendencies over the past 59 years, but with large fluctuations especially found in the time series of R95T. Compared to RX1Day, RX5Day, R95T, and R99T, R10mm and R25mm present severe fluctuations throughout the study period, especially R25mm. The R25mm indicated the number of extremely heavy precipitation days during a year, and presented obviously periodic fluctuations with a significant decreasing trend of 0.02 day yr^{-1} (Figure 7f). In summary, our findings indicated a significant reduction in the number of days with precipitation exceeding 25 mm in the HRB during the period of 1960–2018, with a notable decrease in extremely heavy precipitation days.

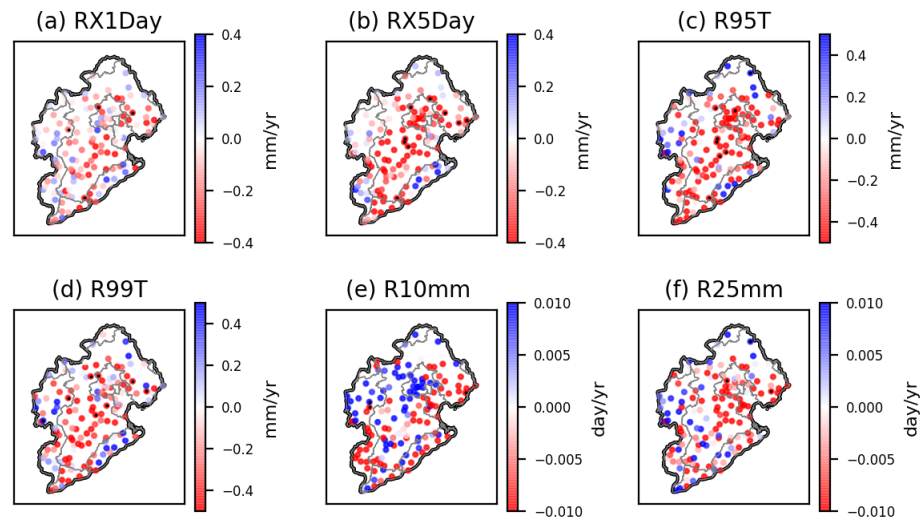


Figure 6. Long-term trends of extreme precipitation indices at gauge stations from 1960 to 2018: (a) RX1Day; (b) RX5Day; (c) R95T; (d) R99T; (e) R10mm; (f) R25mm. The blue circles represent the increasing trends and the red circles represent the decreasing trends. The black dots filled in blue or red circles represent the significance at a confidence level of 95%.

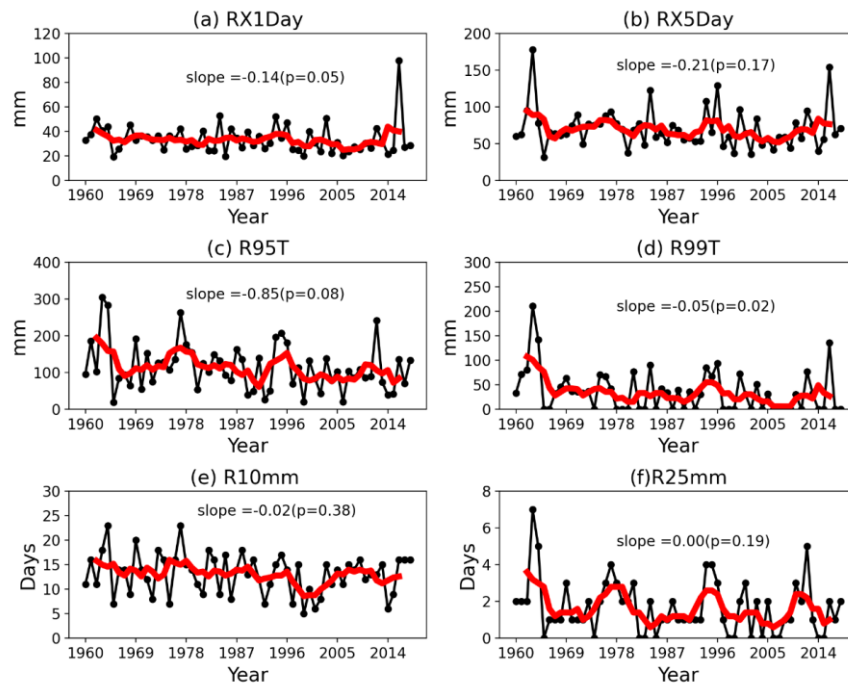


Figure 7. The interannual variability and trends of extreme precipitation indices from 1960 to 2018 in HRB: (a) RX1Day; (b) RX5Day; (c) R95T; (d) R99T; (e) R10mm; (f) R25mm. The black dot line represents the annual time series of precipitation seasonality indices and the thick red line represents the 5-year moving average of each index.

3.4. The Connection between Precipitation Extremes and Precipitation Seasonality

Figures 8 and 9 illustrated a comprehensive analysis of the correlations between precipitation seasonality and extremes at both the basin-wide scale and gauge stations. As shown in Figure 8a–d, the RX1Day, RX5Day, R95T, and R99T represent similar correlation patterns with precipitation seasonality indices: the stations with stronger positive correlations were concentrated in the southwestern part of the HRB, reaching the highest correlation value (0.3) in the southmost part of the HRB. These similar patterns were consistent with the long-term trends of four precipitation extreme indices. However, the strongest connections appeared in the southern part, not in the Beijing or Tianjin administration region where the significant decreasing trends were illustrated.

To further investigate the connection between precipitation seasonality and precipitation extreme indices, the correlation at each gauge station was calculated in Figure 9. RX5Day illustrated the highest correlation with the seasonality index with an R-value of 0.50 ($p = 0.00$). Additionally, R95T and R99T were correlated with the seasonality index with R-values of 0.31 ($p = 0.02$) and 0.35 ($p = 0.01$), respectively. This pattern illustrated that the precipitation extremes were heavily dependent on the precipitation seasonality. The high consistency between the 5-day maximum precipitation and the annual seasonality index highlighted the dependence of the interannual variability in the 5-day maximum precipitation on the precipitation seasonality. Hence, we concluded that the reduced precipitation seasonality corresponded closely to the decreasing precipitation extremes characterized by the maximum 5-day precipitation and extreme wet-day precipitation events.

As shown in Figure 8e,f, the significant connections between precipitation seasonality and R10mm and R25mm were detected, particularly with R25mm, even only among a small number of stations (Figure 6e,f). These connections were demonstrated by the significant positive correlation coefficient, predominantly distributed in the center of the HRB. Hence, the extreme precipitation events within a year were highly dependent on the precipitation seasonality. These connections were further demonstrated in Figure 9e,f by a significantly positive relationship among gauge stations with R-values of 0.27 ($p = 0.04$) and 0.38 ($p = 0.00$). These connections have been also revealed in Figure 6e,f; a decrease in seasonality index slightly induced a lower frequency of R10mm and R25mm. The fluctuations observed in R10 and R25mm were notably dependent on the precipitation seasonality dynamics.

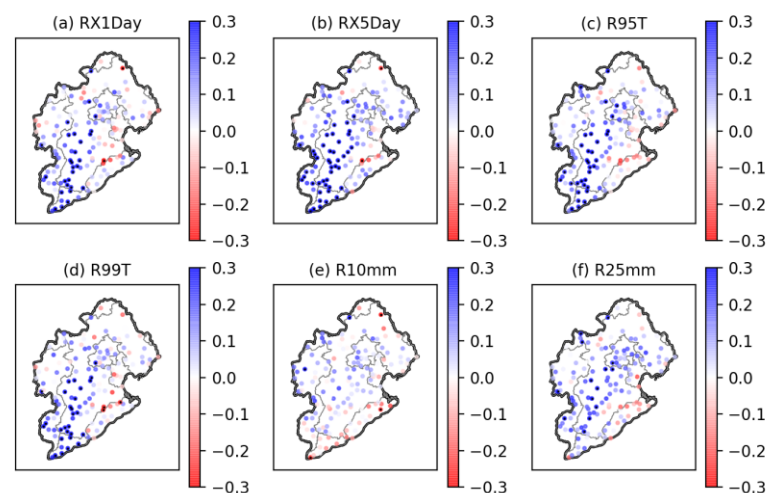


Figure 8. Correlation coefficient of precipitation seasonality indices and extreme precipitation indices in HRB. (a) RX1Day; (b) RX5Day; (c) R95T; (d) R99T; (e) R10mm; (f) R25mm. The blue circles represent the positive correlation and the red circles represent the negative correlation.

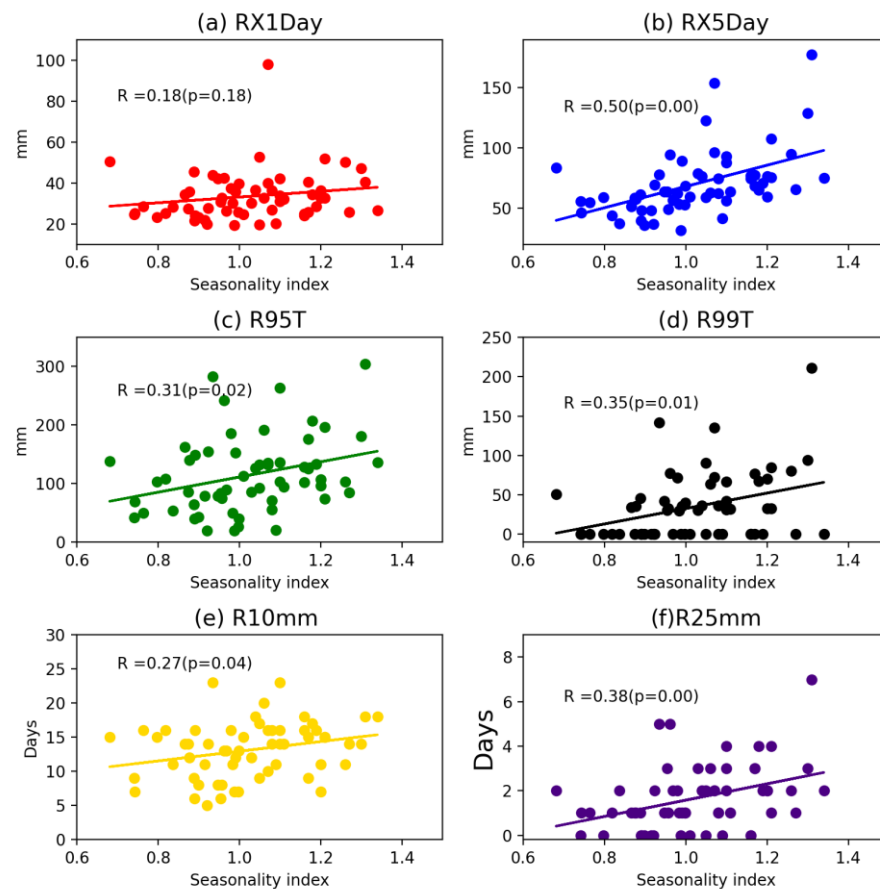


Figure 9. Scatter plot of precipitation seasonality indices and extreme precipitation indices in Hai River basin. The x-axis is the seasonality indices, and y is the extreme precipitation indices: (a) RX1Day; (b) RX5Day; (c) R95T; (d) R99T; (e) R10mm; (f) R25mm.

4. Discussion and Conclusions

Based on the precipitation records from 143 gauge stations in HRB from 1960 to 2018, our study presents a comprehensive study of the climatology, interannual variability, and long-term trends of precipitation seasonality characteristics, including annual magnitude, timing, and duration of wet season, and precipitation seasonality index. We also investigated the possible correlation between precipitation seasonality and precipitation extremes.

Our finding demonstrated a gradual west-to-east delay in the onset dates of the wet season, while the cessation dates of the wet season gradually shifted earlier. Moreover, the duration of the wet season was found to be below 110 days in the eastern basin and over 130 days in the western basin. At the basin-wide scale, a significant trend was observed of an earlier onset date of the wet season (-0.2 day yr^{-1}), along with a significant increase in the duration of the wet season (0.43 day yr^{-1}), accompanied by a slight decrease in annual precipitation during the period of 1960–2018. However, this trend has shown inconsistency with the projected wet season changes over East Asia, an earlier onset and a later cessation of the annual wet season under future climate change [34,36]. The patterns of wet season in the HRB were further supported by the variations and trends in the seasonality index, which exhibited a smooth transition from the western to eastern zones, with a significant decreasing trend (-0.003 yr^{-1}) at the basin-wide scale. Although previous studies have reported moderate and extremely high variabilities in wet seasons [30], the seasonal components of even precipitation extreme events were influenced by the climate variability that showed strong regional variations [32,52,53]. Notably, stations within the Beijing administrative region showed the highest seasonality index with significant decreasing trends. These changes in seasonality index combined with the wet season

duration illustrated that a more evenly precipitation distribution happened over a year in the HRB, especially concentrated in the regions of Metropolises.

Furthermore, our study found that four extreme indices, RX1Day, RX5day, R95T, and R99T, illustrated a similar spatial pattern of long-term trends but varying magnitude. The stations with significant trends in R10mm and R25mm were notably fewer compared to the other four indices. RX1day and R99T revealed significant decreases at rates of $-0.14 \text{ day yr}^{-1}$ ($p = 0.05$) and $-0.05 \text{ day yr}^{-1}$ ($p = 0.02$), respectively. R25mm and R10mm showed no obvious trends over the past 59 years. These findings indicated a significant decrease in the frequency of maximum daily precipitation extreme precipitation events and the number of extremely heavy precipitation days within the HRB from 1960 to 2018. Notably, for the Beijing and Tianjin administration regions, significant decreasing trends were observed in RX1Day (-0.30 mm yr^{-1}), RX5Day (-0.50 mm yr^{-1}), R95T (-0.75 mm yr^{-1}), and R99T (-0.40 mm yr^{-1}), respectively, but increasing trends of R10mm. This phenomenon implied that the heavy precipitation days increased but the extreme heavy precipitation days decreased in the regions of Beijing and Tianjin Area.

Regarding the relationship between precipitation extremes and seasonality, our findings illustrated that RX5Day had the highest correlation with the seasonality index, with an R-value of 0.50 ($p = 0.00$). The R95T and R99T were correlated with the seasonality index with R-values of 0.31 ($p = 0.02$) and 0.35 ($p = 0.01$), respectively. R25mm also showed a strong correlation with the seasonality index, with an R-value of $R = 0.38$ ($p = 0.00$). These patterns suggest that the reduced precipitation seasonality in the HRB was highly influenced by a decrease in maximum 5-day precipitation and extreme wet day precipitation.

In our study, we present a comprehensive spatial–temporal analysis of precipitation seasonality indicators and provide an additional perspective that the precipitation seasonality might partially explain the decreasing trends of precipitation extremes. The precipitation seasonality indicators have been widely used to assess seasonality in many regions where annual rainfall was unevenly distributed and had a unimodal seasonal rainfall distribution [24,41,42,54]. Our study revealed significant correlations between precipitation seasonality and precipitation extremes, supporting the notion that rainfall seasonality is related to the extent of precipitation extremes. This finding was consistent with the previous studies. For instance, Deng et al. [54] observed that the rainfall seasonality decreased in Northeast China from 1961 to 2012, mainly attributed to changes in magnitude and the timing of the arrival of the wet season. Mao et al. [24] found the reduction in precipitation seasonality happened in nine major river basins in China from 1960 to 2018, accompanied by an extended duration of the wet season. Tan et al. [15] illustrated a significant decreasing trend in the precipitation seasonality index among five well-known precipitation datasets in eastern China. As defined, the precipitation seasonality index represents the extent of rainfall concentration during the wet season. Therefore, a reduced seasonality index indicated a more even distribution of precipitation over a year, suggesting a higher occurrence of small and moderate precipitation events and fewer heavy precipitation events during the wet season to form an even distribution of precipitation. This more even distribution reduced the possibility of the heaviest precipitation and precipitation extremes. The significant correlation between precipitation seasonality and precipitation extremes further supports this connection.

Consistently, the significantly decreased frequency of maximum daily precipitation extreme precipitation events and the number of extremely heavy precipitation days were found in HRB between 1960 and 2018. This trend aligned with the overall weakened East Asian monsoon, which led to a reduction in annual rainfall in most parts of China [55,56]. Shao [57] also found that extreme precipitation frequency exhibited a distinctive decreasing trend in the Beijing-Tianjin-Tangshan region from 1950 to 2010. The extreme precipitation frequency and intensity exhibit decreasing trends in North China [58], which was consistent with the results from Xiao et al. [59] and Gu et al. [60].

The precipitation seasonality and precipitation extremes throughout the year were intricately regulated by the variability patterns of precipitation, which were notably in-

fluenced by prevailing large-scale atmospheric circulations [53,59,61]. Notably, the East Asian Summer Monsoon (EASM) exerted a significant impact on the variability and pattern of precipitation in East China, which brought in increasing rainfall in May and led to decreasing rainfall in June [62], resulting in the early arrival of the wet season in the most of China [54]. The EASM's impact extended to a pronounced impact on the monsoon rain belt, fundamentally governing the major rainy season and the rainfall distribution in the wet season of eastern China. The heavy precipitation events are especially closely related to the movement of EASM [21]; Zhang et al. [63] also found a negative correlation between annual precipitation in north plain China and the East Asian Summer Monsoon Index (EASMI). Further, the western Pacific subtropical high (WPSH) was an important component of the EASM system, closely linked to the summer monsoon precipitation pattern in eastern China [64]. The westward expansion of the WPSH contributed to the increasing precipitation in the southeastern part and decreasing precipitation in the northeastern part [21,56,65].

Nevertheless, the EASM was also modulated by large-scale circulation patterns, such as El Niño–Southern Oscillation (ENSO), the North Atlantic Oscillation (NAO), the Pacific Decadal Oscillation (PDO), and the Indian Ocean Dipole (IOD). The ENSO significantly influenced interannual fluctuations and spatial patterns of precipitation seasonality in China, with a close relationship to summer precipitation anomalies [24,66]. In El Niño years, the annual precipitation has a significant increasing trend with an earlier start of the wet season. Total column water vapor in eastern China was higher and moisture convergence appeared in most months, which led to a more even water vapor distribution and a lower precipitation seasonality [24]. The PDO is also an important factor correlated to precipitation, particularly for monsoon regions. The linkage between the warm PDO phase and less summer precipitation in the central part of north China was observed [21,56,67]. Deng et al. [54] found an association between the increase in PDO from 1960 to 2015 and the increased frequency of extreme precipitation in East China. Gu et al. [60] revealed that northeastern China was significantly dominated by northerly winds from dry land during positive NAO, resulting in less water vapor and hence impeding the occurrence of heavy precipitation. The regional responses of annual extreme precipitation intensity and frequency to the large-scale climate indices are different and complex, simultaneously shaped by multiple climate indices at different time phases.

Overall, our study presents a comprehensive analysis of the climatology and the inter-annual variability of precipitation seasonality patterns and their links to the precipitation extremes within the HRB. This research is important for insight into flood and drought control, effective water management, and regional sustainable development. This analysis is of importance, especially to provide a guide for the risk evaluation of urban waterlogging due to extreme precipitation for the metropolis in the basin region, as it has attracted more and more attention in big cities. For future study, the short-duration, like sub-daily extreme event analysis based on a higher-temporal-resolution (like hourly) precipitation dataset is certainly needed, to provide better guidance for updating and improving regulation to handle the short and intense precipitation events. Furthermore, the characteristic and relationship between precipitation seasonality and precipitation extremes at sub-daily or hourly time scale should be explored in future work, especially under urbanization processes of typical urban areas, considering the urban waterlogging risk increased caused by heavy rainfall and posing a significant challenge for mega cities in China.

Author Contributions: All authors contributed to the study's conception and design. X.Z.: original draft. Y.M.: supervision and review. All authors have read and agreed to the published version of the manuscript.

Funding: This research was funded by the National Basic Research Program of China (2020YFA0608201), the National Natural Science Foundation of China (42005127), and the National Basic Research Program of China (No. 2022YFF0801301).

Institutional Review Board Statement: Not applicable.

Informed Consent Statement: Not applicable.

Data Availability Statement: The precipitation data applied in this study are available at <http://data.cma.cn>, accessed on 30 September 2021.

Conflicts of Interest: The authors declare no conflict of interest.

References

1. Elahi, E.; Khalid, Z.; Zhang, Z. Understanding Farmers' Intention and Willingness to Install Renewable Energy Technology: A Solution to Reduce the Environmental Emissions of Agriculture. *Appl. Energy* **2022**, *309*, 118459. [[CrossRef](#)]
2. Abbas, A.; Waseem, M.; Ahmad, R.; Khan, K.A.; Zhao, C.; Zhu, J. Sensitivity Analysis of Greenhouse Gas Emissions at Farm Level: Case Study of Grain and Cash Crops. *Environ. Sci. Pollut. Res.* **2022**, *29*, 82559–82573. [[CrossRef](#)]
3. Elahi, E.; Khalid, Z.; Tauni, M.Z.; Zhang, H.; Lirong, X. Extreme Weather Events Risk to Crop-Production and the Adaptation of Innovative Management Strategies to Mitigate the Risk: A Retrospective Survey of Rural Punjab, Pakistan. *Technovation* **2022**, *117*, 102255. [[CrossRef](#)]
4. Abbas, A.; Zhao, C.; Waseem, M.; Ahmed Khan, K.; Ahmad, R. Analysis of Energy Input–Output of Farms and Assessment of Greenhouse Gas Emissions: A Case Study of Cotton Growers. *Front. Environ. Sci.* **2022**, *9*, 826838.
5. Allen, M.R.; Ingram, W.J. Constraints on Future Changes in Climate and the Hydrologic Cycle. *Nature* **2002**, *419*, 224–232. [[CrossRef](#)] [[PubMed](#)]
6. Asadieh, B.; Krakauer, N.Y. Global Trends in Extreme Precipitation: Climate Models versus Observations. *Hydrol. Earth Syst. Sci.* **2015**, *19*, 877–891. [[CrossRef](#)]
7. Fischer, E.M.; Knutti, R. Observed Heavy Precipitation Increase Confirms Theory and Early Models. *Nat. Clim. Change* **2016**, *6*, 986–991. [[CrossRef](#)]
8. Karl, T.R.; Knight, R.W. Secular Trends of Precipitation Amount, Frequency, and Intensity in the United States. *Bull. Am. Meteorol. Soc.* **1998**, *79*, 231–242. [[CrossRef](#)]
9. Kharin, V.V.; Zwiers, F.W.; Zhang, X.; Wehner, M. Changes in Temperature and Precipitation Extremes in the CMIP5 Ensemble. *Clim. Change* **2013**, *119*, 345–357. [[CrossRef](#)]
10. Marelle, L.; Myhre, G.; Hodnebrog, Ø.; Sillmann, J.; Samset, B.H. The Changing Seasonality of Extreme Daily Precipitation. *Geophys. Res. Lett.* **2018**, *45*, 11-352–11-360. [[CrossRef](#)]
11. Min, S.-K.; Zhang, X.; Zwiers, F.W.; Hegerl, G.C. Human Contribution to More-Intense Precipitation Extremes. *Nature* **2011**, *470*, 378–381. [[CrossRef](#)] [[PubMed](#)]
12. Guerreiro, S.B.; Fowler, H.J.; Barbero, R.; Westra, S.; Lenderink, G.; Blenkinsop, S.; Lewis, E.; Li, X.-F. Detection of Continental-Scale Intensification of Hourly Rainfall Extremes. *Nat. Clim. Change* **2018**, *8*, 803–807. [[CrossRef](#)]
13. Pachauri, R.K.; Allen, M.R.; Barros, V.R.; Broome, J.; Cramer, W.; Christ, R.; Church, J.A.; Clarke, L.; Dahe, Q.D.; Dasgupta, P.; et al. *Climate Change 2014 Synthesis Report. Contribution of Working Groups I, II, and III to the Fifth Assessment Report of the Intergovernmental Panel on Climate Change*; IPCC: Geneva, Switzerland, 2014; ISBN 978-92-9169-143-2.
14. Prein, A.F.; Liu, C.; Ikeda, K.; Trier, S.B.; Rasmussen, R.M.; Holland, G.J.; Clark, M.P. Increased Rainfall Volume from Future Convective Storms in the US. *Nat. Clim. Change* **2017**, *7*, 880–884. [[CrossRef](#)]
15. Tan, X.; Wu, Y.; Liu, B.; Chen, S. Inconsistent Changes in Global Precipitation Seasonality in Seven Precipitation Datasets. *Clim. Dyn.* **2020**, *54*, 3091–3108. [[CrossRef](#)]
16. Seneviratne, S.I.; Zhang, X.; Adnan, M.; Badi, W.; Dereczynski, C.; Di Luca, A.; Ghosh, S.; Iskandar, I.; Kossin, J.; Lewis, S.; et al. Weather and Climate Extreme Events in a Changing Climate. In *Climate Change 2021: The Physical Science Basis. Contribution of Working Group I to the Sixth Assessment Report of the Intergovernmental Panel on Climate Change*; Masson-Delmotte, V., Zhai, P., Pirani, A., Connors, S.L., Péan, C., Berger, S., Caud, N., Chen, Y., Goldfarb, L., Gomis, M.I., et al., Eds.; Cambridge University Press: Cambridge, UK; New York, NY, USA, 2021; pp. 1513–1766.
17. Zhang, Y.; Wang, K. Global Precipitation System Scale Increased from 2001 to 2020. *J. Hydrol.* **2023**, *616*, 128768. [[CrossRef](#)]
18. Dankers, R.; Arnell, N.W.; Clark, D.B.; Falloon, P.D.; Fekete, B.M.; Gosling, S.N.; Heinke, J.; Kim, H.; Masaki, Y.; Satoh, Y.; et al. First Look at Changes in Flood Hazard in the Inter-Sectoral Impact Model Intercomparison Project Ensemble. *Proc. Natl. Acad. Sci. USA* **2014**, *111*, 3257–3261. [[CrossRef](#)] [[PubMed](#)]
19. Hammond, M.J.; Chen, A.S.; Djordjević, S.; Butler, D.; Mark, O. Urban Flood Impact Assessment: A State-of-the-Art Review. *Urban Water J.* **2015**, *12*, 14–29. [[CrossRef](#)]
20. Milly, P.C.D.; Wetherald, R.T.; Dunne, K.A.; Delworth, T.L. Increasing Risk of Great Floods in a Changing Climate. *Nature* **2002**, *415*, 514–517. [[CrossRef](#)]
21. Wu, Y.; Ji, H.; Wen, J.; Wu, S.-Y.; Xu, M.; Tagle, F.; He, B.; Duan, W.; Li, J. The Characteristics of Regional Heavy Precipitation Events over Eastern Monsoon China during 1960–2013. *Glob. Planet. Change* **2019**, *172*, 414–427. [[CrossRef](#)]
22. Westra, S.; Alexander, L.V.; Zwiers, F.W. Global Increasing Trends in Annual Maximum Daily Precipitation. *J. Clim.* **2013**, *26*, 3904–3918. [[CrossRef](#)]
23. Hu, W.; Yao, J.; He, Q.; Chen, J. Changes in Precipitation Amounts and Extremes across Xinjiang (Northwest China) and Their Connection to Climate Indices. *PeerJ* **2021**, *9*, e10792. [[CrossRef](#)] [[PubMed](#)]

24. Mao, Y.; Wu, G.; Xu, G.; Wang, K. Reduction in Precipitation Seasonality in China from 1960 to 2018. *J. Clim.* **2022**, *35*, 227–248. [[CrossRef](#)]
25. Fu, G.; Yu, J.; Yu, X.; Ouyang, R.; Zhang, Y.; Wang, P.; Liu, W.; Min, L. Temporal Variation of Extreme Rainfall Events in China, 1961–2009. *J. Hydrol.* **2013**, *487*, 48–59. [[CrossRef](#)]
26. Wu, G.; Li, Z.; Fu, C.; Zhang, X.; Zhang, R.; Zhang, R.; Zhou, T.; Li, J.; Li, J.; Zhou, D.; et al. Advances in Studying Interactions between Aerosols and Monsoon in China. *Sci. China Earth Sci.* **2016**, *59*, 1–16. [[CrossRef](#)]
27. Zhai, P.; Zhang, X.; Wan, H.; Pan, X. Trends in Total Precipitation and Frequency of Daily Precipitation Extremes over China. *J. Clim.* **2005**, *18*, 1096–1108. [[CrossRef](#)]
28. Wood, R. Role of Mean and Variability Change in Changes in European Annual and Seasonal Extreme Precipitation Events. *Earth Syst. Dyn.* **2023**, *14*, 797–816. [[CrossRef](#)]
29. Gu, X.; Ye, L.; Xin, Q.; Zhang, C.; Zeng, F.; Nerantzaki, S.D.; Papalexiou, S.M. Extreme Precipitation in China: A Review on Statistical Methods and Applications. *Adv. Water Resour.* **2022**, *163*, 104144. [[CrossRef](#)]
30. Pendergrass, A.G.; Knutti, R.; Lehner, F.; Deser, C.; Sanderson, B.M. Precipitation Variability Increases in a Warmer Climate. *Sci. Rep.* **2017**, *7*, 17966. [[CrossRef](#)] [[PubMed](#)]
31. Wood, R.; Lehner, F.; Pendergrass, A.; Schlunegger, S. Changes in Precipitation Variability across Time Scales in Multiple Global Climate Model Large Ensembles. *Environ. Res. Lett.* **2021**, *16*, 084022. [[CrossRef](#)]
32. van der Wiel, K.; Bintanja, R. Contribution of Climatic Changes in Mean and Variability to Monthly Temperature and Precipitation Extremes. *Commun. Earth Environ.* **2021**, *2*, 1. [[CrossRef](#)]
33. Biasutti, M.; Sobel, A.H. Delayed Sahel Rainfall and Global Seasonal Cycle in a Warmer Climate. *Geophys. Res. Lett.* **2009**, *36*, L23707. [[CrossRef](#)]
34. Dwyer, J.G.; Biasutti, M.; Sobel, A.H. The Effect of Greenhouse Gas-Induced Changes in SST on the Annual Cycle of Zonal Mean Tropical Precipitation. *J. Clim.* **2014**, *27*, 4544–4565. [[CrossRef](#)]
35. Marvel, K.; Biasutti, M.; Bonfils, C.; Taylor, K.E.; Kushnir, Y.; Cook, B.I. Observed and Projected Changes to the Precipitation Annual Cycle. *J. Clim.* **2017**, *30*, 4983–4995. [[CrossRef](#)]
36. Song, F.; Leung, L.R.; Lu, J.; Dong, L. Seasonally Dependent Responses of Subtropical Highs and Tropical Rainfall to Anthropogenic Warming. *Nat. Clim. Change* **2018**, *8*, 787–792. [[CrossRef](#)]
37. Seth, A.; Rauscher, S.A.; Biasutti, M.; Giannini, A.; Camargo, S.J.; Rojas, M. CMIP5 Projected Changes in the Annual Cycle of Precipitation in Monsoon Regions. *J. Clim.* **2013**, *26*, 7328–7351. [[CrossRef](#)]
38. Darwish, M.M.; Fowler, H.J.; Blenkinsop, S.; Tye, M.R. A Regional Frequency Analysis of UK Sub-Daily Extreme Precipitation and Assessment of Their Seasonality. *Int. J. Climatol.* **2018**, *38*, 4758–4776. [[CrossRef](#)]
39. Deng, S.; Sheng, C.; Yang, N.; Song, L.; Huang, Q. Anthropogenic Forcing Enhances Rainfall Seasonality in Global Land Monsoon Regions. *Environ. Res. Lett.* **2020**, *15*, 104057. [[CrossRef](#)]
40. Livada, I.; Asimakopoulos, D.N. Individual Seasonality Index of Rainfall Regimes in Greece. *Clim. Res.* **2005**, *28*, 155–161. [[CrossRef](#)]
41. Feng, X.; Porporato, A.; Rodriguez-Iturbe, I. Changes in Rainfall Seasonality in the Tropics. *Nat. Clim. Change* **2013**, *3*, 811–815. [[CrossRef](#)]
42. Pascale, S.; Lucarini, V.; Feng, X.; Porporato, A.; ul Hasson, S. Analysis of Rainfall Seasonality from Observations and Climate Models. *Clim. Dyn.* **2015**, *44*, 3281–3301. [[CrossRef](#)]
43. Xia, J.; Liu, C.; Ren, G. Opportunity and Challenge of the Climate Change Impact on the Water Resource of China. *Adv. Earth Sci.* **2011**, *26*, 1–12.
44. Ren, Z.; Xiong, A. Operational system development on three-step quality control of observations from AWS (in Chinese). *Meteorol. Mon.* **2007**, *33*, 19–24.
45. Cao, L.; Zhu, Y.; Tang, G.; Yuan, F.; Yan, Z. Climatic Warming in China According to a Homogenized Data Set from 2419 Stations. *Int. J. Climatol.* **2016**, *36*, 4384–4392. [[CrossRef](#)]
46. Wu, G.; Li, Y.; Qin, S.; Mao, Y.; Wang, K. Precipitation Unevenness in Gauge Observations and Eight Reanalyses from 1979 to 2018 over China. *J. Clim.* **2021**, *34*, 9797–9810. [[CrossRef](#)]
47. Wu, G.; Qin, S.; Huang, C.; Ma, Z.; Shi, C. Seasonal Precipitation Variability in Mainland China Based on Entropy Theory. *Int. J. Climatol.* **2021**, *41*, 5264–5276. [[CrossRef](#)]
48. Basso, B.; Martinez-Feria, R.A.; Rill, L.; Ritchie, J.T. Contrasting Long-Term Temperature Trends Reveal Minor Changes in Projected Potential Evapotranspiration in the US Midwest. *Nat. Commun.* **2021**, *12*, 1476. [[CrossRef](#)] [[PubMed](#)]
49. Berner, L.T.; Massey, R.; Jantz, P.; Forbes, B.C.; Macias-Fauria, M.; Myers-Smith, I.; Kumpula, T.; Gauthier, G.; Andreu-Hayles, L.; Gaglioti, B.V.; et al. Summer Warming Explains Widespread but Not Uniform Greening in the Arctic Tundra Biome. *Nat. Commun.* **2020**, *11*, 4621. [[CrossRef](#)]
50. Perkins-Kirkpatrick, S.E.; Lewis, S.C. Increasing Trends in Regional Heatwaves. *Nat. Commun.* **2020**, *11*, 3357. [[CrossRef](#)]
51. Wang, J.; Chen, Y.; Tett, S.F.B.; Yan, Z.; Zhai, P.; Feng, J.; Xia, J. Anthropogenically-Driven Increases in the Risks of Summertime Compound Hot Extremes. *Nat. Commun.* **2020**, *11*, 528. [[CrossRef](#)] [[PubMed](#)]
52. Pal, I.; Anderson, B.T.; Salvucci, G.D.; Gianotti, D.J. Shifting Seasonality and Increasing Frequency of Precipitation in Wet and Dry Seasons across the U.S. *Geophys. Res. Lett.* **2013**, *40*, 4030–4035. [[CrossRef](#)]

53. Mallakpour, I.; Villarini, G. Investigating the Relationship between the Frequency of Flooding over the Central United States and Large-Scale Climate. *Adv. Water Resour.* **2016**, *92*, 159–171. [[CrossRef](#)]
54. Deng, S.; Yang, N.; Li, M.; Cheng, L.; Chen, Z.; Chen, Y.; Chen, T.; Liu, X. Rainfall Seasonality Changes and Its Possible Teleconnections with Global Climate Events in China. *Clim. Dyn.* **2019**, *53*, 3529–3546. [[CrossRef](#)]
55. Li, F.; Zhang, G.; Xu, Y.J. Spatiotemporal Variability of Climate and Streamflow in the Songhua River Basin, Northeast China. *J. Hydrol.* **2014**, *514*, 53–64. [[CrossRef](#)]
56. Zhu, Y.; Wang, H.; Zhou, W.; Ma, J. Recent Changes in the Summer Precipitation Pattern in East China and the Background Circulation. *Clim. Dyn.* **2011**, *36*, 1463–1473. [[CrossRef](#)]
57. Shao, Z. *The New Urban Area Development: A Case Study in China*; Springer: Berlin/Heidelberg, Germany, 2015.
58. Deng, Y.; Jiang, W.; He, B.; Chen, Z.; Jia, K. Change in Intensity and Frequency of Extreme Precipitation and Its Possible Teleconnection With Large-Scale Climate Index Over the China From 1960 to 2015. *J. Geophys. Res. Atmos.* **2018**, *123*, 2068–2081. [[CrossRef](#)]
59. Xiao, C.; Wu, P.; Zhang, L.; Song, L. Robust Increase in Extreme Summer Rainfall Intensity during the Past Four Decades Observed in China. *Sci. Rep.* **2016**, *6*, 38506. [[CrossRef](#)] [[PubMed](#)]
60. Gu, X.; Zhang, Q.; Singh, V.P.; Shi, P. Non-Stationarities in the Occurrence Rate of Heavy Precipitation across China and Its Relationship to Climate Teleconnection Patterns. *Int. J. Climatol.* **2017**, *37*, 4186–4198. [[CrossRef](#)]
61. Hoerling, M.; Eischeid, J.; Perlwitz, J.; Quan, X.-W.; Wolter, K.; Cheng, L. Characterizing Recent Trends in U.S. Heavy Precipitation. *J. Clim.* **2016**, *29*, 2313–2332. [[CrossRef](#)]
62. Kajikawa, Y.; Yasunari, T.; Yoshida, S.; Fujinami, H. Advanced Asian Summer Monsoon Onset in Recent Decades. *Geophys. Res. Lett.* **2012**, *39*, L03803. [[CrossRef](#)]
63. Zhang, D.; Wang, T.; Liu, Y.; Zhang, S.; Meng, X. Spatial and Temporal Characteristics of Annual and Seasonal Precipitation Variation in Shijiazhuang Region, North China. *Environ. Earth Sci.* **2021**, *80*, 656. [[CrossRef](#)]
64. Huang, Y.; Wang, H.; Fan, K.; Gao, Y. The Western Pacific Subtropical High after the 1970s: Westward or Eastward Shift? *Clim. Dyn.* **2015**, *44*, 2035–2047. [[CrossRef](#)]
65. Yu, R.; Zhou, T. Seasonality and Three-Dimensional Structure of Interdecadal Change in the East Asian Monsoon. *J. Clim.* **2007**, *20*, 5344–5355. [[CrossRef](#)]
66. Chen, W.; Feng, J.; Wu, R. Roles of ENSO and PDO in the Link of the East Asian Winter Monsoon to the Following Summer Monsoon. *J. Clim.* **2013**, *26*, 622–635. [[CrossRef](#)]
67. Qian, C.; Zhou, T. Multidecadal Variability of North China Aridity and Its Relationship to PDO during 1900–2010. *J. Clim.* **2014**, *27*, 1210–1222. [[CrossRef](#)]

Disclaimer/Publisher’s Note: The statements, opinions and data contained in all publications are solely those of the individual author(s) and contributor(s) and not of MDPI and/or the editor(s). MDPI and/or the editor(s) disclaim responsibility for any injury to people or property resulting from any ideas, methods, instructions or products referred to in the content.